ChemPubSoc Europe

DOI: 10.1002/cctc.201600221

CHEMCATCHEM Communications

# Mesoporous High-Surface-Area Copper–Tin Mixed-Oxide Nanorods: Remarkable for Carbon Monoxide Oxidation

Honggen Peng,[a, b] Yang Liu,[a] Yarong Li,[a] Xianhua Zhang,[a] Xianglan Tang,[a] Xianglan Xu,[a] Xiuzhong Fang,[a] Wenming Liu,[a] Ning Zhang,[a] and Xiang Wang*[a]

Mesoporous, high-surface-area Cu–Sn mixed-oxide nanorods were fabricated for the first time by nanocasting with the use of mesoporous KIT-6 silica as the hard template. The Cu–Sn nanorods are significantly more active than 1% Pd/$SnO_2$ for the oxidation of CO and possesses long-term durability and potent water resistance; they thus have the potential to replace noble metal catalysts for emission-control processes.

The morphology of a catalyst is critical for its catalytic performance; therefore, morphology control has become a popular strategy to improve the activity, selectivity, and stability of a catalyst over recent years.[1–9] Metal-oxide catalysts with an elongated rod-shape structure have many advantages, including high surface to volume ratio, preferentially exposed active facets, and good mechanical stability, which are key factors that are used to determine the application potential of the catalysts.[6,10–12] Shen and co-workers[13] reported that $Co_3O_4$ nanorods not only catalyze CO oxidation at temperature as low as −77 °C but also remain very stable in a moisture stream. $MnO_2$ nanorods prepared by the hydrothermal method have also been shown to have much better catalytic performance for toluene combustion than their polycrystalline powder counterpart prepared by the precipitation method.[14] Rod-like $CeO_2$ has been studied as a support for Au and NiO to prepare catalysts for the preferential oxidation of CO in a $H_2$-rich gas[4] and for the selective reduction of NO with $NH_3$,[15] respectively, and both catalysts show improved reaction performance compared with $CeO_2$ polyhedra and pure NiO. In addition, it was reported that Mn–Ce mixed-oxide nanorods with a high Mn content also display very high activity and stability for toluene combustion.[16]

Our group previously reported that the activity of pure $SnO_2$ nanorods for CO oxidation is much improved relative to that of other morphologies.[17] Most importantly, their catalytic behavior is similar to that of supported noble metal catalysts. Although the specific surface area of this $SnO_2$ nanorod catalyst is as low as 1 $m^2g^{-1}$ and even though it does not contain any active oxygen species, it has preferentially exposed [1 1 0] facets, which have been shown by other researchers to be the active facets,[17] but the activity of this $SnO_2$ nanorod catalyst is still lower than that of the comparison sample 1% Pd/$SnO_2$. If its activity can be further improved, the $SnO_2$ nanorod catalyst itself could be a good candidate to replace noble metal catalysts. Very recently, mesoporous $SnO_2$ and Cu–Sn mixed-oxide nanosheets were successfully prepared by our group, and they showed superior activity and stability for CO oxidation at low temperature owing to the presence of a large amount of mobile oxygen species and their high surface areas.[18] The creation of mesopores in the $SnO_2$ nanorods could increase their surface area, produce mobile oxygen species, and enhance the contact of the reactants with the active sites, which would thus eventually improve the activity of the catalyst so that performance competitive with that of noble metals could be achieved. Nanocasting technology is a versatile method to create non-siliceous nanostructured porous materials.[19] In a casting process, a replica structure can usually be obtained, which is the negative replica. Until now, to the best of our knowledge, there is little research on the use of mesoporous silica as a hard template to prepare mesoporous mixed-oxide nanorods through a nanocasting strategy.

In this communication, a mesoporous silica, KIT-6, with ordered mesopores (Figures S1–S3, Supporting Information) was synthesized and used for the first time as the hard template to prepare Cu–Sn metal-oxide nanorods with a Cu/Sn molar ratio of 1:1 through nanocasting,[19–21] and the resulting catalyst was used for CO oxidation after calcination at different temperatures. The detailed preparation procedures and the reaction condition are described in the Supporting Information.

The SEM and TEM images in Figure 1 demonstrate that the Cu–Sn mixed oxide calcined at different temperatures has rod-like morphology. Upon increasing the temperature from 300 to 400 °C, the nanorod becomes elongated and neater. However, a further increase in the calcination temperature to 550 °C clearly induces the formation of some polycrystalline metal-oxide powder, which indicates that part of the rod structure becomes damaged at higher temperatures. As shown in the TEM images in Figure 1 d, on the Cu–Sn nanorod calcined at 400 °C, some mesopores are present, and this was further confirmed by the $N_2$ adsorption/desorption results shown in Figure S4. As listed in Table S1, the three samples calcined at different temperatures have similar pore sizes, which are approxi-

[a] Dr. H. Peng, Y. Liu, Y. Li, X. Zhang, X. Tang, Dr. X. Xu, Dr. X. Fang, Prof. Dr. W. Liu, Prof. Dr. N. Zhang, Prof. Dr. X. Wang
Institute of Applied Chemistry, College of Chemistry
Nanchang University
Nanchang, Jiangxi 330031 (China)
E-mail: xwang23@ncu.edu.cn

[b] Dr. H. Peng
School of Chemistry and Chemical Engineering
Shanghai Jiao Tong University
800 Dongchuan Road, Shanghai 200240 (China)

Supporting Information and the ORCID identification number(s) for the author(s) of this article can be found under http://dx.doi.org/10.1002/cctc.201600221.

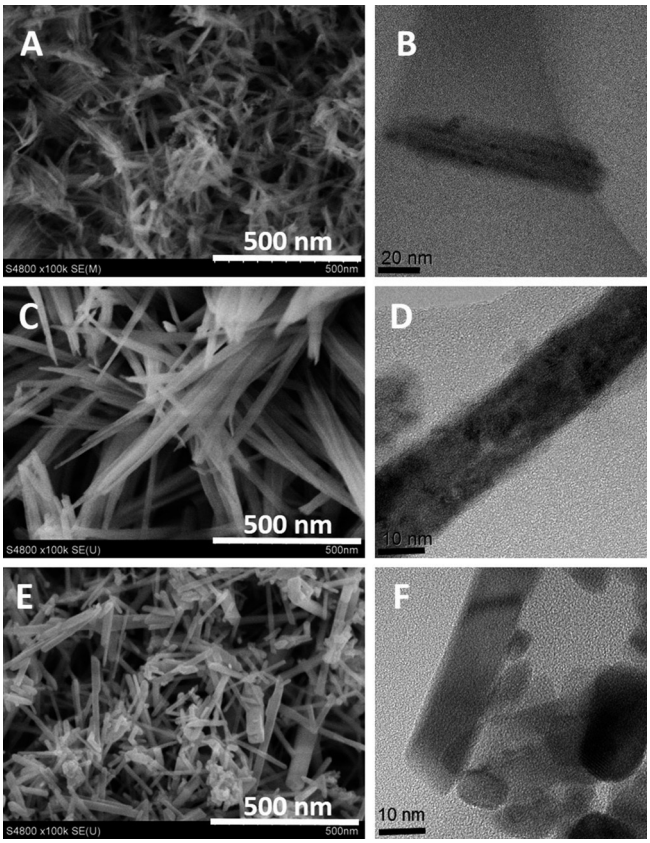


**Figure 1.** SEM (left) and TEM (right) images of Cu–Sn nanorods (molar ratio of Cu:Sn = 1:1) calcined at a, b) 300 °C, c, d) 400 °C, and e, f) 550 °C.

mately 4 nm. Owing to the formation of the mesoporous structure, the surface areas of all three samples are above 110 $m^2 g^{-1}$, which is much larger than the surface area of the unmodified $SnO_2$ nanorod prepared previously by our group by using the molten salt method.[17] Apparently, the mesoporous structure and high surface area are favorable for the activity of the catalysts.

Usually, by using mesoporous silica as the hard template and the metal oxide as precursor, after removing the template by NaOH or HF, a replica of the metal oxide is obtained by using the nanocasting method. However, as reported in this communication, a novel mesoporous mixed-oxide nanorod was formed by using the nanocasting method. From the TEM images of the Cu–Sn mixed-oxide nanorods, the size of the cross section of the rods is approximately 10 nm, which is very similar to the pore size of KIT-6 (average pore size is 7.8 nm, Figure S2), so the rod-shape structure might be formed by the metal precursor grown along the main cylindrical pores of KIT-6 (Figure S1 c), though KIT-6 is a bicontinuous cubic *Ia3d* mesosilica.

To elucidate the phase compositions of the Cu–Sn nanorods, the XRD patterns of the samples were compared with the individual $SnO_2$ and CuO species (Figure S5). All the Cu–Sn nanorods clearly show the diffraction features of the tetragonal rutile $SnO_2$ phase, which indicates that a major part of the Cu cations could have been incorporated into its lattice to form a solid solution structure.[18,22] To confirm this, the $2\theta$ and $d$ values of the two strongest peaks of the rutile $SnO_2$ phase, peaks (1 1 0) and (1 0 1), in the Cu–Sn nanorod samples were carefully identified and are compared in Table S2. As previously reported,[23,24] $Cu^{2+}$ with a coordination number (CN) of 6 has a radius of 0.074 nm, whereas that of $Sn^{4+}$ with the same CN is 0.069 nm. In comparison with individual $SnO_2$, the two diffraction peaks are shifted to lower angles but the $d$ values increase, which testifies to the expansion of the distance between the crystal facets by incorporation of larger $Cu^{2+}$ cations into the crystal lattice of $SnO_2$. Indeed, this further proves that a considerable amount of the Cu cations was introduced into the $SnO_2$ lattice to form a solid solution structure. However, the valence state difference between the two cations is large. As a result, the $Cu^{2+}$ cations can only be dissolved into the $SnO_2$ lattice with a certain capacity.[25] With a Cu/Sn molar ratio of 1:1, the amount of Cu cations clearly exceeds the capacity. Therefore, the $Cu(OH)_2$ phase is observed for the CuSn-rod-300 sample, and CuO is observed for the CuSn-rod-400 and CuSn-rod-550 samples as the minor phases. Notably, upon increasing the calcination temperature, the mean crystallite size of the $SnO_2$ phase becomes larger, which indicates better crystallization of the formed Cu–Sn solid solution.

To further clarify the formation of a solid solution structure between the Cu and Sn oxides, CuSn-rod-400, the typical catalyst in this study, was thus measured by high angle annular dark field (HAADF) scanning transmission electron microscopy (STEM) mapping, and the image is shown in Figure 2. The mapping zone is labeled in the SEM image in Figure 2 a, whereas the elemental distribution of the Cu, Sn, and O elements is displayed in Figure 2 b–d. The three elements are distributed very uniformly in the sample, which confirms that

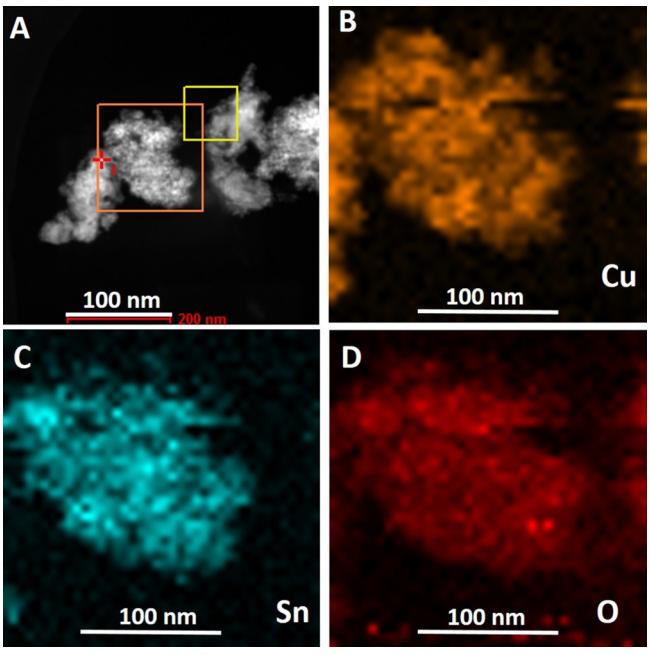


**Figure 2.** a) HAADF STEM image and b–d) elemental mapping of mesoporous Cu–Sn nanorods (molar ratio of Cu/Sn = 1:1) calcined at 400 °C in air.

**Table 1.** Redox behavior and reaction performance of mesoporous CuSn nanorod catalysts.[a]

| Sample | $H_2$ consumption [mmol $g^{-1}$] | | | | $O_{ads}/O_{lat}$ | Reaction rate [$10^{-4}$ mmol $g^{-1}$ $s^{-1}$] | Reaction rate [$10^{-6}$ mmol $m^{-2}$ $s^{-1}$] | $E_a$[b] [kJ $mol^{-1}$] |
|---|---|---|---|---|---|---|---|---|
| | < 240 °C | ≈380 °C | > 530 °C | Total | (XPS) | | | |
| CuSn-rod-300 | 2.5 | 0.7 | 5.7 | 8.9 | 0.6 | 0.3 | 0.114 | 66.5 |
| CuSn-rod-400 | 3.8 | 1.1 | 3.8 | 8.7 | 2.7 | 9.2 | 5.9 | 47.3 |
| CuSn-rod-550 | 3.6 | 0.8 | 3.6 | 8.0 | 1.5 | 4.9 | 4.3 | 50.3 |

[a] Molar ratio of Cu/Sn = 1:1. [b] Activation Energy.

a homogeneous solid solution structure is formed in the Cu–Sn mixed-oxide nanorods.

The redox properties of the samples were studied by temperature-programmed reduction by hydrogen ($H_2$-TPR), and the profiles are shown in Figure S6; the $H_2$ uptake amount is quantified in Table 1. For all the Cu–Sn nanorod samples calcined at different temperatures, three groups of reduction peaks can be distinctly observed below 240 °C, at approximately 380 °C, and above 540 °C. The peak below 240 °C is assigned to the reduction of CuO species in the samples into metallic Cu.[18] In contrast, the peak above 530 °C is assigned to the reduction of $SnO_2$ to metallic Sn,[17] whereas the small peak at approximately 380 °C is believed to be the reduction of deficient oxygen species induced by the formation of the Cu–Sn solid solution structure in the samples.[18] Upon varying the calcination temperature, the reduction behavior of the samples is clearly changed. For low-temperature CO oxidation, the oxygen species reduced at low temperature are believed to be critical for the activity of the catalyst if it follows the Mars–van Krevlen mechanism.[26] Whereas the total amount of $H_2$ consumed by the samples decreases from 8.9 to 8.0 mmol $g^{-1}$, the amounts consumed by the samples at the first two low-temperature peaks are 3.2, 4.9, and 4.4 mmol $g^{-1}$ for the CuSn-rod-300, CuSn-rod-400, and CuSn-rod-550 samples, respectively. Apparently, CuSn-rod-400, the sample calcined at 400 °C, clearly consumes the largest amount of hydrogen at approximately 240 and 380 °C, which indicates that this sample contains the largest amount of active oxygen species, which are believed to be favorable for CO oxidation. In comparison, CuSn-rod-300, the sample calcined at 300 °C, possesses the lowest amount of these active oxygen species, possibly as a result of the still presence of a large quantity of OH groups.

X-ray photoelectron spectroscopy (XPS) was adopted to identify the surface composition of the catalysts, and the spectra are displayed in Figure S7. The binding energies observed in Figure S7 a,b for Cu 2p and Sn 3d are typical for $Cu^{2+}$ and $Sn^{4+}$,[18] which is in line with the $H_2$-TPR results. The asymmetric O 1s peaks of the samples shown in Figure S7 c indicate the presence of surface oxygen species with different chemical environments. Therefore, the O 1s peaks of the samples were deconvoluted, as shown in Figure S7 d–f. Whereas the peak at a binding energy (BE) of approximately 530 eV is assigned to surface lattice oxygen ($O_{lat}$),[27] the peak at a BE of approximately 532 eV is attributed to loosely bonded surface oxygen species ($O_{ads}$),[27] which is believed to be important for the oxidation activity of the catalysts. Therefore, the $O_{ads}/O_{lat}$ ratios of the samples were quantified and are listed in Table 1. Apparently, the CuSn-rod-400 sample possesses the highest value, which further testifies to that fact that this sample has the largest amount of active oxygen vacancies. Indeed, the XPS results are in agreement with what was detected by the $H_2$-TPR experiments.

The activity of the catalysts was evaluated by CO oxidation. As shown in Figure 3 a, CuSn-rod-400, the sample calcined at 400 °C, displays the highest overall activity, on which complete CO conversion occurred at 130 °C. In comparison with the pure $SnO_2$ nanorod prepared by us, this temperature is 130 °C lower.[17] Furthermore, its overall activity is even higher than that of 1% Pd/$SnO_2$, the comparison catalyst, which achieves complete CO oxidation at 140 °C (Figure 3 a). It is clear that with the combination of Cu and Sn oxides, Cu–Sn nanorods with activity higher than that of supported Pd can be obtained.

Even though CuSn-rod-300, the sample calcined at 300 °C, has the highest surface area among the three samples, it exhibits the lowest overall activity, which indicates that the surface area is not the determining factor for the activity of the catalysts. To elucidate the inherent reasons accounting for the activity, the differential rates on the samples were collected and are plotted as Arrhenius plots in Figure 3 b. Although CuSn-rod-400 and CuSn-rod-550 evidently have lower surface areas than CuSn-rod-300, they have significantly higher reaction rates under differential conditions. For easy comparison, the differential rate at 100 °C for each sample is listed in Table 1 together with the overall activation energy. The two samples calcined at higher temperatures not only have higher rates but also have lower activation energies. This strongly indicates that more reactive sites are formed in these two catalysts. As described above, XRD phase analysis indicates that on CuSn-rod-300, the $Cu(OH)_2$ phase is detected instead of the CuO phase because of the low calcination temperature. It is reasonable to deduce that in this sample, a large amount of OH groups are still present, which could influence the effective formation of the solid solution structure, as testified by less shifting of the $2\theta$ and $d$ values. As a result, a smaller amount of active oxygen species is formed, as evidenced by the $H_2$-TPR and XPS results. In contrast, upon increasing the calcination temperature to 400 °C, a larger amount of active oxygen species is produced, but these species will be partly destroyed upon increasing the temperature further to 550 °C owing to better crystallization. As a consequence, CuSn-rod-400, the

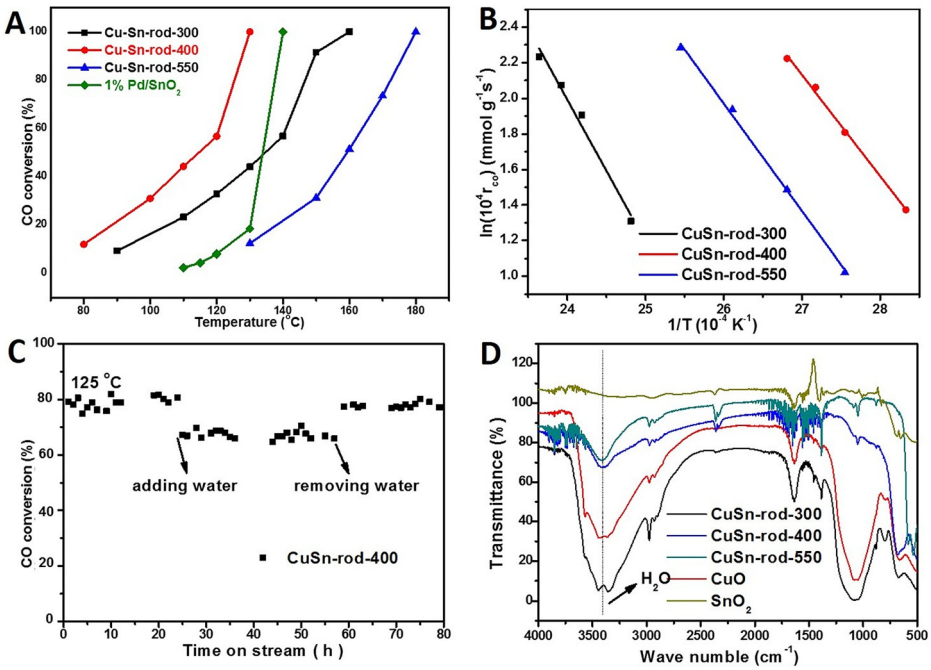


**Figure 3.** a) CO conversion versus reaction temperatures, b) Arrhenius plots, c) stability test in the absence and presence of water vapor, and d) FTIR spectra of the Cu–Sn nanorod samples (molar ratio of Cu/Sn = 1:1) after water adsorption.

sample calcined at 400 °C, displays the highest activity among all the samples.

In real exhaust, 5–10% water vapor is generally present; therefore, CuSn-rod-400, the optimal catalyst in this study, was subjected to a long-term stability test in the absence and presence of 5% water vapor. As shown in Figure 3c, after the addition of 5% water vapor, the CO conversion decreases by approximately 10%, but the conversion can be completely restored after removing the water vapor. Not only does this indicate that CuSn-rod-400 is stable, but it also indicates that CuSn-rod-400 is water resistant. FTIR spectroscopy was thus used to investigate the water adsorption behavior of the samples, and the spectra are shown in Figure 3d. After saturation in water vapor, followed by purging by He flow to remove any physically adsorbed water, whereas pure CuO displays an evident water adsorption band at approximately $\tilde{\nu} = 3350\ cm^{-1}$, the individual $SnO_2$ does not show any adsorption of water.[27] Notably, owing to the initial presence of a large amount of OH groups in its structure, CuSn-rod-300 displays a big band at $\tilde{\nu} = 3350\ cm^{-1}$. However, although CuSn-rod-400 and CuSn-rod-550 also display water adsorption bands at the same wavenumbers, their integrated areas are much smaller than that of pure CuO, and thus, the combination of Cu and Sn oxides can produce catalysts with significantly improved water tolerance.

In summary, mesoporous, high-surface-area Cu–Sn mixed-oxide nanorods were successfully fabricated by using mesoporous silica (KIT-6) as the hard template for the first time. Cu cations were incorporated into the crystal lattice of rutile $SnO_2$ to form a solid solution structure, which induced the formation of more active oxygen species. CuSn-rod-400, the nanorod sample calcined at 400 °C, displayed the highest activity for CO oxidation and was even more active than a comparison Pd catalyst (1% $Pd/SnO_2$) under the same conditions. Last but not least, the Cu–Sn nanorod catalysts also showed superior stability and water resistance, and thus they are potential replacements for precious metal catalysts for real exhaust cleaning.

## Experimental Section

### Synthesis of mesoporous silica KIT-6 hard template

The mesoporous silica template with cubic *Ia3d* bicontinuous structure (KIT-6) was prepared according to the literature.[1,2] Typically, P123 (9 g, $EO_{20}PO_{70}EO_{20}$, $Mw = 5800$, Aldrich) was dissolved in distilled deionized water (326 g) and concentrated HCl (17.7 g, ≈35–37%). Then, butanol (9 g, >99%) was added under constant stirring at 35 °C. After stirring for approximately 1 h, tetraethyl orthosilicate (TEOS; 19.4 g, 98%) was added to the above solution. The mixture was continuously stirred for another 24 h at 35 °C and was subsequently transferred into a 500 mL Teflon-lined stainless-steel autoclave and heated at 100 °C for 24 h under static conditions. The white precipitate recovered by filtration was thoroughly washed with distilled deionized water, which was followed by drying at 90 °C overnight. P123 was removed by calcining the as-made materials at 550 °C for 6 h in air.

### Synthesis of mesoporous Cu–Sn nanorods by nanocasting

Typically, $Cu(NO_3)_2{\cdot}3H_2O$ (3.02 g, 12.5 mmol) and $SnCl_4{\cdot}5H_2O$ (4.38 g, 12.5 mmol) were dissolved in absolute ethanol (10 mL) and then KIT-6 (2.5 g, calcined at 200 °C under vacuum) was added. The mixture was stirred for 1 h at room temperature. Afterwards, the temperature was increased to 60 °C, and continuous stirring was maintained until the solvent was fully evaporated. The powder was dried at 60 °C for 12 h and then calcined at 200 °C for 4 h at a heat-

ing rate of 1 °C min$^{-1}$. The above procedure was repeated except that the solution mixture consisted of $Cu(NO_3)_2 \cdot 3H_2O$ (1 g), $SnCl_4 \cdot 5H_2O$ (1.5 g), and absolute ethanol (5 mL). The obtained sample was then calcined at 300, 400, or 550 °C for 4 h. After this, the silica template (KIT-6) was removed with an aqueous 2 M NaOH solution at 65 °C for 6 h. This etching step was repeated to ensure that the silica template was completely removed. The sample was then dried thoroughly at 90 °C overnight. The final sample was named CuSn-rod-300, CuSn-rod-400, or CuSn-rod-550, respectively. The elemental compositions of the samples were determined by inductively coupled plasma (ICP), and the results are listed in Table S1. For the samples calcined at 400 and 550 °C, the Cu/Sn molar ratios were approximately 1:1, as designed. However, for the sample calcined at 300 °C, part of the Cu species was lost during the etching process owing to the low calcination temperature, which resulted in a Cu/Sn molar ratio of 0.81.

### Catalyst characterization

The powder X-ray diffraction (XRD) patterns were recorded with a Bruker AXS D8Focus diffractometer operating at 40 kV and 30 mA with $CuK_\alpha$ irradiation ($\lambda = 1.5405$ Å). Scans were taken with a $2\theta$ range from 10 to 90° for wide angle scan with a step of 5° min$^{-1}$ and from 0.5 to 6° for small angle scan with a step of 1° min$^{-1}$. To keep the data comparable, all of the samples were tested continuously under the same conditions. The mean crystallite sizes of the samples were calculated with the Scherrer equation on the basis of the three strongest peaks of $SnO_2$ with *hkl* of (1 1 0), (1 0 1), and (2 1 1). The calculated experimental error for $2\theta$ measurement of the peaks was ±0.01°, which ensured reliable identification of peak shift observed by solid solution formation. The copper and tin contents were determined by inductively coupled plasma atomic emission spectroscopy (ICP-AES) with an IRIS Intrepid II XSP instrument (Thermo Electron Corporation).The scanning electron microscopy (SEM) images were taken with a Hitachi S-4800 field emission scanning electron microscope. Transmission electron microscopy (TEM) images were taken with a Tecnai F30 transmission electron microscope. The high angle annular dark field scanning transition electron microscopy (HAADF-STEM) images, elemental phase mapping, and surface scans by energy-dispersive spectroscopy were also obtained by using a Tecnai F30 transmission electron microscope equipped with an Oxford EDX detector operated at 300 keV. Nitrogen adsorption/desorption of the samples was performed at 77 K with an ASAP2020 instrument. The specific surface areas of the samples were calculated by using the Brunauer–Emmett–Teller (BET) method in the relative pressure ($P/P_0$) range of 0.05 to 0.25. The pore-size distributions of the samples were calculated with the Barrett–Joyner–Halenda (BJH) method. The average pore sizes of the samples were obtained from the peak positions of the distribution curves. The total pore volume of each catalyst was accumulated at a relative pressure of $P/P_0 = 0.99$. Hydrogen temperature programmed reduction ($H_2$-TPR) experiments were performed with a FINESORB 3010C instrument in a 30 mL min$^{-1}$ 10% $H_2$/Ar gas mixture flow. Generally, 50 mg of the catalyst was used for the tests. Prior to the experiments, the catalysts were recalcined in a high purity air flow at 300 °C for 30 min to remove any surface impurities. The temperature was then increased from room temperature to 850 °C at a rate of 10 °C min$^{-1}$. A thermal conductivity detector (TCD) was employed to monitor $H_2$ consumption. For $H_2$ consumption quantification, CuO (99.99%) was used as the calibration standard. X-ray photoelectron spectroscopy (XPS) was performed with a PerkinElmer PHI1600 system by using a single MgK X-ray source operating at 300 W and 15 kV. The spectra were obtained at ambient temperature with an ultrahigh vacuum. The binding energies were calibrated by using the C 1s peak of graphite at a binding energy of 284.5 eV as a reference. FTIR spectra were recorded in the 500–4000 cm$^{-1}$ range with a Nicolet Nexus 670 FTIR spectrometer in absorbance mode at a spectral resolution of 2 cm$^{-1}$ at room temperature. To measure the water adsorption, the fresh samples were saturated in water vapor prior to the experiments and were subsequently purged by an ultrahigh purity He flow for 30 min to remove any physically adsorbed water.

### Activity evaluation

The catalytic performance of the catalysts was evaluated by CO oxidation with a U-shaped quartz tube (ID = 6 mm) reactor with a down flow over 100 mg catalyst. Typically, 0.3–0.4 mm catalyst particles were used for activity test. A K-type thermocouple was placed on top of the catalyst bed with the thermocouple head point touching the catalyst to monitor the reaction temperature. To measure the light-off behaviors of the catalysts, all data were collected with increasing temperature. The volume composition of the feed gas was 1% CO, 21% $O_2$, and balanced by high-purity $N_2$, with a flow rate of 40 mL min$^{-1}$, which corresponds to a space velocity of 24 000 mL h$^{-1}$ g$_{cat}^{-1}$). The reactants and products were analyzed on-line with a GC9310 gas chromatograph equipped with a TDX-01 column and a TCD detector. To obtain steady-state kinetic data, the reaction at each temperature was stabilized at least 30 min before analysis. The flow rate of the $H_2$ carrier gas was 30 mL min$^{-1}$.

## Acknowledgements

*This work was supported by the National Natural Science Foundation of China (21263015, 21567016, and 21503106), the Education Department of Jiangxi Province (KJLD14005), and the Natural Science Foundation of Jiangxi Province (20142BAB213013, 20151BAB203024, and 20151BBE50006), which is greatly acknowledged by the authors.*

**Keywords:** copper · mesoporous materials · nanostructures · oxidation · tin

[1] W. Huang, Y. Gao, *Catal. Sci. Technol.* **2014**, *4*, 3772 – 3784.
[2] T. Nguyen, C. Dinh, T. Do, *Chem. Commun.* **2015**, *51*, 624 – 635.
[3] Z. Dou, C. Cao, Y. Chen, W. Song, *Chem. Commun.* **2014**, *50*, 14889 – 14891.
[4] G. Yi, Z. Xu, G. Guo, K. Tanaka, Y. Yuan, *Chem. Phys. Lett.* **2009**, *479*, 128 – 132.
[5] Y. Li, W. Shen, *Chem. Soc. Rev.* **2014**, *43*, 1543 – 1574.
[6] P. Hu, M. E. Schuster, Z. Huang, F. Xu, S. Jin, Y. Chen, W. Hua, D. S. Su, X. Tang, *Chem. Eur. J.* **2015**, *21*, 9619 – 9623.
[7] A. Pendashteh, S. E. Moosavifard, M. S. Rahmanifar, Y. Wang, M. F. El-Kady, R. B. Kaner, M. F. Mousavi, *Chem. Mater.* **2015**, *27*, 3919 – 3926.
[8] F. Wang, H. Dai, J. Deng, G. Bai, K. Ji, Y. Liu, *Environ. Sci. Technol.* **2012**, *46*, 4034 – 4041.
[9] H. Kim, J. Cho, *J. Mater. Chem.* **2008**, *18*, 771 – 775.
[10] G. Chen, Q. Xu, Y. Yang, C. Li, T. Huang, G. Sun, S. Zhang, D. Ma, X. Li, *ACS Appl. Mater. Interfaces* **2015**, *7*, 23538 – 23544.
[11] S. Zhang, C. Chang, Z. Huang, Y. Ma, W. Gao, J. Li, Y. Qu, *ACS Catal.* **2015**, *5*, 6481 – 6488.
[12] S. Zhuo, J. Zhang, Y. Shi, Y. Huang, B. Zhang, *Angew. Chem. Int. Ed.* **2015**, *54*, 5693 – 5696; *Angew. Chem.* **2015**, *127*, 5785 – 5788.
[13] X. Xie, Y. Li, Z. Liu, M. Haruta, W. Shen, *Nature* **2009**, *458*, 746 – 749.

[14] F. Shi, F. Wang, H. Dai, J. Dai, J. Deng, Y. Liu, G. Bai, K. Ji, C. T. Au, *Appl. Catal. A* **2012**, *433 – 434*, 206 – 213.
[15] P. Maitarad, J. Han, D. Zhang, L. Shi, S. Namuangruk, T. Rungrotmongkol, *J. Phys. Chem. C* **2014**, *118*, 9612 – 9620.
[16] Y. Liao, M. Fu, L. Chen, J. Wu, B. Huang, D. Ye, *Catal. Today* **2013**, *216*, 220 – 228.
[17] X. Wang, L. Xiao, H. Peng, W. Liu, X. Xu, *J. Mater. Chem. A* **2014**, *2*, 5616 – 5619.
[18] Y. Li, H. Peng, X. Xu, Y. Peng, X. Wang, *RSC Adv.* **2015**, *5*, 25755 – 25764.
[19] A. H. Lu, F. Schüth, *Adv. Mater.* **2006**, *18*, 1793 – 1805.
[20] D. Gu, F. Schuth, *Chem. Soc. Rev.* **2014**, *43*, 313 – 344.
[21] B. Tian, X. Liu, H. Yang, S. Xie, C. Yu, B. Tu, D. Zhao, *Adv. Mater.* **2003**, *15*, 1370 – 1374.
[22] M. J. Fuller, M. E. Warwick, *J. Chem. Soc. Chem. Commun.* **1973**, 210a.
[23] X. Xu, R. Zhang, X. Zeng, X. Han, Y. Li, Y. Liu, X. Wang, *ChemCatchem* **2013**, *5*, 2025 – 2036.
[24] M. Luo, J. Ma, J. Lu, Y. Song, Y. Wang, *J. Catal.* **2007**, *246*, 52 – 59.
[25] X. Xu, F. Liu, X. Han, Y. Wu, W. Liu, R. Zhang, N. Zhang, X. Wang, *Catal. Sci. Technol.* **2016**, DOI:10.1039/c5cy01870f, in press.
[26] Y. Liu, H. Dai, Y. Du, J. Deng, L. Zhang, Z. Zhao, C. T. Au, *J. Catal.* **2012**, *287*, 149 – 160.
[27] X. Xu, X. Sun, H. Han, H. Peng, W. Liu, X. Peng, X. Wang, X. Yang, *Appl. Surf. Sci.* **2015**, *355*, 1254 – 1260.

Received: February 24, 2016
Revised: April 15, 2016
Published online on June 15, 2016